Switchable Band Topology and Geometric Current in Sliding Bilayer Elemental Ferroelectric

Zhuang Qian[1,2], Zhihao Gong[3], Jian Li[1,2], Hua Wang[4*], and Shi Liu[1,2,*]

[1]*Department of Physics, School of Science, Hangzhou 310030, China*
[2]*Institute of Natural Sciences, Westlake Institute for Advanced Study, Hangzhou 310024, China*
[3]*Academy of Interdisciplinary Studies on Intelligent Molecules, Tianjin Key Laboratory of Structure and Performance for Functional Molecules, College of Chemistry, Tianjin Normal University, Tianjin 300387, China*
[4]*Center for Quantum Matter, School of Physics, Zhejiang University, Hangzhou 310058, China*

(Received 26 May 2025; accepted manuscript online 3 June 2025)

We demonstrate that the sliding motion between two layers of the newly discovered ferroelectric and topologically trivial bismuth (Bi) monolayer [*Nature* **617** 67 (2023)] can induce a sequence of topological phase transitions, alternating between $\mathbb{Z}_2$ trivial and nontrivial states. The lateral shift, while preserving spatial symmetry, can switch the quantum spin Hall state on and off. The sliding-induced changes in out-of-plane atomic buckling, which are directly coupled to in-plane ferroelectricity, are shown to significantly modulate the band gap and drive the topological phase transitions. We map out the topological phase diagram and in-plane ferroelectricity with respect to sliding displacements. With appropriate sliding, the bismuth bilayer can transition into a nontrivial polar metal, exhibiting a pronounced shift current response arising from interband geometric quantities of electronic bands. Moreover, bilayer Bi supports a sliding-tunable nonlinear anomalous Hall response resulting from the geometric Berry curvature dipole. Configurations that are $\mathbb{Z}_2$ nontrivial can generate drastically different transverse currents orthogonal to the external electric field, as both the direction and magnitude of the Berry curvature dipole at the Fermi level are highly sensitive to the sliding displacement. Our results suggest that bilayer bismuth, with its ability to generate multiple types of geometric currents, offers a versatile platform for power-efficient "Berry slidetronics" for multistate memory applications integrating both band topology and ferroelectricity.

DOI: 10.1088/0256-307X/42/7/070715 CSTR: 32039.14.0256-307X.42.7.070715

Two-dimensional (2D) van der Waals (vdW) materials have garnered significant attention in the fields of condensed matter physics and materials science.[1–5] Their unique properties, such as highly tunable electronic properties and remarkable mechanical flexibility, position them as promising candidates for a myriad of applications, ranging from next-generation electronics and optoelectronics to energy storage and flexible devices.[6–13] The layers in these materials are held together by weak vdW forces, making them particularly susceptible to twisting and sliding. Such structural deformations, especially twisting, can profoundly alter the electronic behaviors of 2D materials.[14–16] For example, adjusting the twist angle between adjacent layers results in the formation of long-wavelength moiré superlattices. The moiré potential with a modulation period much larger than the atomic lattice constant can quench the kinetic energy of electrons and effectively enhance the electronic correlation, setting the stage for various quantum phenomena, including Hofstadter butterfly patterns,[17,18] superconductivity,[14,19,20] Mott insulators,[21–23] and moiré excitons.[24,25]

Recent studies have demonstrated that interlayer sliding can induce out-of-plane polarization in bilayer systems, even when they are composed of nonpolar monolayers.[26–28] This phenomenon is attributed to changes in the layer stacking configuration caused by sliding, which leads to a reversal in the direction of charge transfer between the layers and consequently switchable out-of-plane polarization.[26] Notable bilayer systems possessing sliding ferroelectricity that have been confirmed experimentally are bilayer graphene and transition metal dichalcogenides.[29–32] Unlike twisting, sliding in bilayers of identical monolayers generally has a less significant impact on their electronic and optical properties, as it does not significantly modulate the periodic potential landscape. One notable exception, predicted theoretically, occurs in sliding bilayer graphene, where the electronic topological transition involving pair annihilations of massless Dirac fermions is sensitively influenced by the direction of the lateral interlayer shift.[33] However, sliding-induced electronic topological transitions,[34] such as the $\mathbb{Z}_2$ topological phase transition, are rarely reported in gapped 2D materials. This scarcity is not particularly surprising. A $\mathbb{Z}_2$ topological phase transition, characterized by a change in the band structure's topology, demands the closure of the band gap, wherein the conduction and valence bands

*Corresponding authors. Email: daodaohw@zju.edu.cn; liushi@westlake.edu.cn
© 2025 Chinese Physical Society and IOP Publishing Ltd. All rights, including for text and data mining, AI training, and similar technologies, are reserved.

must touch at least at one point in the momentum space. The intrinsic inert response of the band gap to sliding naturally hinders the transition between a trivial insulator and a topological insulator.

Topological insulators typically exhibit larger dipole transition matrix elements and enhanced Berry curvature compared to trivial insulators,[35] making them promising candidates for Berry curvature memory.[36] This memory concept leverages the geometric Berry curvature dipole-induced nonlinear anomalous Hall effect, providing a novel mechanism for data storage and manipulation. In particular, Berry curvature memory, deriving its functionality from the topological properties of materials, could offer advantages in terms of speed, energy efficiency, and durability over conventional semiconductor memory technologies.[36–39] In this context, a sliding-induced $\mathbb{Z}_2$ topological phase transition represents a compelling opportunity. Such a mechanism, if achievable, could act as an additional control knob, unlocking novel functionalities and device types.

In this study, we utilize first-principles density functional theory (DFT) calculations, including hybrid functionals, to demonstrate that sliding motion between two layers of the newly discovered single-element ferroelectric bismuth (Bi) monolayer triggers successive trivial-to-nontrivial topological phase transitions.[40,41] We find that, although the Bi monolayer is topologically trivial, stacking it into a bilayer and applying appropriate sliding can transform it into a quantum spin Hall insulator. This stands in sharp contrast with previous studies of bilayer systems where the monolayer itself is already topologically nontrivial.[42–44] Removing the requirement for a nontrivial monolayer to achieve a switchable topological phase expands the materials design space for topological materials. The sliding-tunable band gap and the ensuing quantum phase transition in the ferroelectric Bi bilayer could enable energy-efficient mechanical switching between on and off states of a quantum spin Hall insulator, along with its quantized edge conductance. An intriguing aspect is that the significant modulation of the band gap and the resulting band inversion arise primarily from changes in out-of-plane atomic buckling driven by interlayer sliding. This buckling strongly influences the charge transfer process, thereby profoundly altering the electronic structure. We have constructed a topological phase diagram as a function of in-plane sliding motions of various magnitudes along all possible directions, providing a precise map for the fine-tuning of quantum states. Additionally, we show that $\mathbb{Z}_2$ nontrivial states induced by different magnitudes of sliding motions can generate nonlinear Hall currents that vary in both direction and magnitude. This suggests another sliding-tunable current, in addition to the symmetry-protected edge current. We further demonstrate that interlayer sliding can transform the Bi layer into a nontrivial topological polar metal, characterized by a pronounced shift current response.[45] We propose that bilayer bismuth may serve as a promising platform for the realization of power-efficient "Berry slidtronics", harnessing both deterministically controllable ferroelectricity, band topology, and geometric current for nonvolatile multistate memory applications.

All plane-wave DFT calculations are performed using Quantum Espresso.[46,47] The vdW bilayers are fully optimized using a generalized gradient approximation of the Perdew–Burke–Ernzerhof (PBE) type,[48] augmented with Grimme dispersion corrections, and employing Garrity–Bennett–Rabe–Vanderbilt ultrasoft pseudopotentials.[49] We use a plane-wave kinetic energy cutoff of 50 Ry, a charge density cutoff of 250 Ry, a $12 \times 12 \times 1$ Monkhorst–Pack k-point mesh for Brillouin zone (BZ) integration, an ionic energy convergence threshold of 10^{-5} Ry, and a force convergence threshold of 10^{-4} Ry to converge the structural parameters. A sufficiently large vacuum of 50 Å is used to minimize image interactions arising from the periodic boundary conditions. For band structure calculations, the spin–orbit coupling (SOC) is taken into account at the fully relativistic level with norm-conserving pseudopotentials provided by the PseudoDoJo project,[50] in combination with energy cutoffs of 80 Ry and 320 Ry for the wavefunction and charge density, respectively. Additionally, we compute the electronic structure employing the Heyd–Scuseria–Ernzerhof (HSE) hybrid functional[51] with a $4 \times 4 \times 1$ q-point grid during the self-consistent-field cycles. The HSE band structure is obtained through Wannier interpolation[52] using Wannier90[53] interfaced with Quantum Espresso. The topological state is determined by computing the $\mathbb{Z}_2$ topological index using the Wilson loop method, based on the Wannier tight-binding Hamiltonians constructed with Wannier90.

The structure of ferroelectric bismuth monolayer in the space group of $Pmn2_1$ can be viewed as a distorted, phosphorene-like structure. The presence of out-of-plane atomic buckling (h) breaks the inversion symmetry, leading to a spontaneous charge disproportion between neighboring Bi atoms and an in-plane polarization along the y-axis.[54] Xu *et al.* have recently confirmed experimentally the switchable in-plane polarization in this single-element 2D material.[40] The bilayer configuration studied in this work consists of one monolayer stacked directly atop another [see Fig. 1(a)], giving rise to ferroelectric coupling between the in-plane polarizations of the individual monolayers. In this vertically stacked configuration that preserves the symmetry of the individual monolayers, the lattice vectors $(\boldsymbol{a}, \boldsymbol{b})$ of the upper layer are oriented parallel to those of the lower layer. Upon sliding the upper layer relative to the lower one, the sliding vector is defined as $\boldsymbol{d}_\mathrm{s} = u_x\boldsymbol{a} + u_y\boldsymbol{b}$, with the resulting configuration labeled as $\mathcal{S}[u_x, u_y]$. For example, considering the sliding vector $\boldsymbol{d}_\mathrm{s} = 0.4\boldsymbol{a}$, as shown in Fig. 1(b), the configuration is denoted as $\mathcal{S}[0.4, 0.0]$. We note that the presence of a mirror symmetry $\mathcal{M}_x$ in the monolayer renders configuration $\mathcal{S}[u_x, u_y]$ equivalent to $\mathcal{S}[1-u_x, u_y]$. For the initial bilayer configuration ($\mathcal{S}[0.0, 0.0]$), both the lattice constants and atomic positions are fully optimized. For the sliding configuration, atomic positions along the z-axis are allowed to relax. Additionally, sliding in this bilayer configuration does not break the out-of-plane inversion symmetry, thereby preventing the emergence of sliding ferroelectricity featuring interlayer charge transfer-induced out-of-plane polarization.

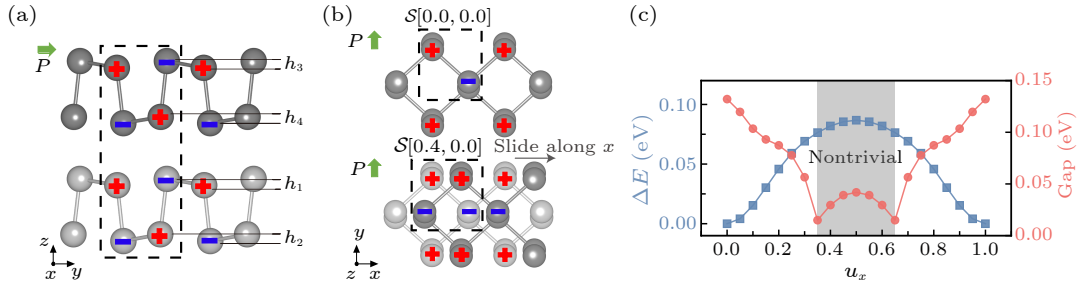

Fig. 1. Schematics of the (a) side and (b) top views of bilayer bismuth that has one monolayer stacked directly atop another. The positive and negative Bader charges are labeled with + and − signs respectively, with in-plane polarization (green arrow) along the y-axis. The out-of-plane atomic buckling (h) is responsible for the in-plane ferroelectricity. The Bi atoms in the upper layer are colored black, while those in the lower layer are gray. Top view of configuration $\mathcal{S}[0.0, 0.0]$ (top) and configuration $\mathcal{S}[0.4, 0.0]$ (bottom), with the upper layer shifted by $\boldsymbol{d}_s = 0.4\boldsymbol{a}$. (c) Evolution of energy and direct gap as a function of u_x. The gray area represents the $\mathbb{Z}_2$ topological nontrivial region.

We present the relative PBE energies of various configurations during sliding along the x-axis, relative to the initial configuration in Fig. 1(c). The sliding process significantly modulates the PBE band gap. Specifically, the direct band gap continuously decreases with increasing u_x, and the bilayer transitions into a topologically nontrivial phase at configuration $\mathcal{S}[0.4, 0.0]$. For $0.35 < u_x < 0.65$, all configurations are nontrivial, with the direct band gap first increasing and then decreasing. Further sliding beyond this range drives the system back into a topologically trivial regime. It is worth noting that, although the topologically nontrivial configurations are slightly higher in energy, they could be stabilized through mechanical clamping of the sliding displacement.[55] Additionally, we have also calculated the configurations where all atomic positions are relaxed and can obtain localized metastable states, which are topologically nontrivial, such as the configuration $\mathcal{S}[0.5, 0.0]$ (see details in Supplementary Materials).

Based on our benchmark calculations comparing HSE+SOC and PBE+SOC, we find that both methods predict similar band structures (see details in Supplementary Materials). Therefore, we map out the topological state of bilayer Bi as a function of sliding defined by u_x and u_y. In Fig. 2(a), a heatmap is designed to concurrently illustrate the topological state and the magnitude of the layer-averaged atomic buckling, defined as $\langle h \rangle = (h_1 + h_2 + h_3 + h_4)/4$. In this heatmap, a value of "0" denotes a $\mathbb{Z}_2$ trivial state, and a "1" indicates a nontrivial state. The intensity of the background color corresponds to the magnitude of $\langle h \rangle$, which also reflects the degree of in-plane asymmetry, as the in-plane ferroelectricity of the Bi monolayer arises from the out-of-plane corrugation height. The heatmap reveals that distinct sliding vectors result in significantly different values of $\langle h \rangle$, highlighting the sensitivity of the system to sliding displacements. A strong correlation is observed between band topology and $\langle h \rangle$. Sliding configurations with $\langle h \rangle \approx 0$ exhibit anti-ferroelectric coupling between the in-plane polarizations of the upper and lower layers, and these configurations are consistently topologically trivial. Conversely, configurations with larger atomic buckling amplitudes tend to exhibit topologically nontrivial states. Overall, the heatmap unveils a complex landscape of topological phase transitions induced by in-plane sliding. A cluster of configurations displaying nontrivial band topology coalesces into a distinctive butterfly-shaped region, with its center at $\mathcal{S}[0.5, 0.0]$. Notably, an outlier state at $\mathcal{S}[0.2, 0.5]$ is nontrivial, anomalously nestled within a cluster of trivial states.

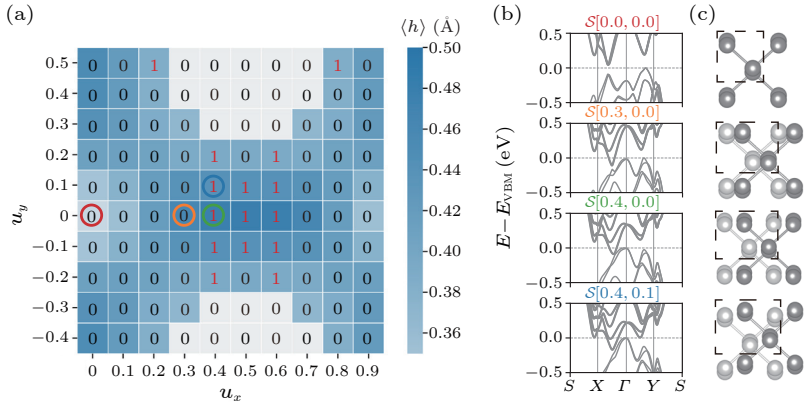

Fig. 2. (a) Heatmap of topological states of bilayer bismuth in configuration $\mathcal{S}[u_x, u_y]$, with "0" and "1" representing $\mathbb{Z}_2$ trivial and nontrivial band topology, respectively. The background color scales with the value of the layer-averaged buckling height $\langle h \rangle = (h_1 + h_2 + h_3 + h_4)/4$ defined in Fig. 1. (b) Band structures of configurations $\mathcal{S}[0.0, 0.0]$, $\mathcal{S}[0.3, 0.0]$, $\mathcal{S}[0.4, 0.0]$, and $\mathcal{S}[0.4, 0.1]$, highlighted in (a), with their top views shown in (c). The valence band maximum (VBM) is chosen as the reference energy when plotting the band structure.

The heatmap provides a convenient visual tool to design sliding pathways to fine-tune quantum states. Figure 2(b) presents the band structures of four representative configurations shown in Fig. 2(a). The starting configuration of bilayer Bi, $\mathcal{S}[0.0, 0.0]$, is a semiconductor with a direct band gap of approximately 0.133 (0.174) eV, as predicted by PBE+SOC (HSE+SOC). At a sliding distance of $u_x = 0.35$, the gap is almost closed. Subsequent sliding along x to $u_x = 0.4$ reopens the band gap. It is confirmed with both HSE+SOC and PBE+SOC that before the gap closure, bilayer Bi configurations like $\mathcal{S}[0, 0]$ and $\mathcal{S}[0.3, 0]$ are trivial insulators with $\mathbb{Z}_2 = 0$, whereas $\mathcal{S}[0.4, 0]$ is a topological insulator featuring a direct band gap E_g of 0.03 eV and $\mathbb{Z}_2 = 1$. It is clear that sliding along the x-axis for one lattice vector induces sequential trivial-nontrivial-trivial topological phase transitions.

We perform a series of model calculations to investigate the relationship between band topology and buckling height. Taking the configuration $\mathcal{S}[0.5, 0.1]$ as an example, it exhibits topologically nontrivial properties at its optimized ground state. By manually varying the buckling height, we examine its impact on the band gap and $\mathbb{Z}_2$ topological invariant, with the results shown in Fig. 3. For a fixed sliding vector $\boldsymbol{d}_s = 0.5\boldsymbol{a} + 0.1\boldsymbol{b}$, the system is topologically nontrivial only within an optimal range of buckling heights, specifically when $0.23 < \langle h \rangle < 0.46$ Å. Outside this range, the system undergoes topological phase transitions. For instance, the band gap closes near $\langle h \rangle = 0.46$ Å, and the direct gap increases as the buckling height increases, rendering the system topologically trivial. Similarly, when $\langle h \rangle < 0.23$ Å, the direct gap also increases as the buckling height decreases, again leading to a topologically trivial state. These results highlight the highly nonlinear relationship between the direct gap and the buckling height. Our findings suggest that the sliding-induced topological phase transition in the Bi bilayer is driven by the modulation of atomic buckling. Since the buckling height directly correlates with the in-plane polarization, the Bi bilayer represents a system where band topology is directly coupled to ferroelectricity.

The Bi bilayer, with its sliding-tunable ferroelectricity, band topology, and metallicity, offers a unique platform for investigating geometric currents driven by both interband and intraband geometric quantities of electronic bands. Notably, the in-plane polarization in bilayer Bi breaks the inversion symmetry, thereby intrinsically

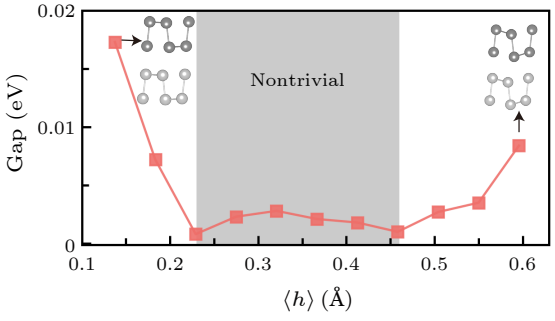

Fig. 3. Dependence of direct band gap and band topology on the buckling height $\langle h \rangle$ in the configuration $\mathcal{S}[0.5, 0.1]$.

capable of generating shift current.[56,57] This current is a nonlinear photocurrent generated in non-centrosymmetric materials and is intimately related to the interband Berry connection and the shift vector. The shift current tensor is derived as

$$\sigma^{abb}(0;\omega,-\omega) = -\frac{\mathrm{i}\pi e^3}{2\hbar^2}\int\frac{\mathrm{d}\boldsymbol{k}}{8\pi^3}\sum_{nm} f_{nm}R^{a,b}_{nm}r^{b}_{nm}r^{b}_{mn}\delta(\omega_{mn}-\omega), \quad (1)$$

where $R^{a,b}_{nm} = \frac{\partial\phi^b_{nm}}{\partial k^a} - \mathcal{A}^a_n - \mathcal{A}^a_m$ is the shift vector with $\mathcal{A}^a_n = \mathrm{i}\langle n|\partial k^a|n\rangle$ the intraband Berry connection, and $r^b_{nm} = |r^b_{nm}|\mathrm{e}^{-\mathrm{i}\phi^b_{nm}}$ is the interband Berry connection with ϕ_{nm} being the phase factor. Meanwhile, by leveraging intraband geometric properties, such as Berry curvature associated with nontrivial states, it becomes possible to induce a nonlinear anomalous Hall current[58] in bilayer Bi when it is in the polar metal state. Unlike the conventional Hall effect, which requires the breaking of time-reversal symmetry and scales linearly with the applied electric field $\mathcal{E}$, the nonlinear Hall current manifests as a second-order response to $\mathcal{E}$. In the nonlinear anomalous Hall effect, the induced geometric current in the static limit flows perpendicular to the electric field and exhibits a quadratic dependence on field strength, as expressed by

$$j^0_a = \chi_{abc}\mathcal{E}_b\mathcal{E}^*_c\,. \quad (2)$$

Here, the nonlinear conductivity tensor χ_{abc} is given by[59,60]

$$\chi_{abc} = -\epsilon_{adc}\frac{\mathrm{e}^3\tau}{2(1+\mathrm{i}\omega\tau)}D_{bd}\,, \quad (3)$$

where ϵ_{adc} is the Levi-Civita tensor, τ is the relaxation time, and ω is the frequency of the applied external field, with $\mathcal{E}_c(\omega) = \mathcal{E}_c\mathrm{e}^{\mathrm{i}\omega t}$. The nonlinear conductivity plays a crucial role and is intimately connected to the Berry curvature dipole D, with the primary contribution originating from states near the Fermi surface. The specific form of the Berry curvature dipole D_{bd} is expressed as

$$D_{bd} = \sum_n\int_k f^0_n(\partial_b\Omega^d_n) = -\sum_n\int_k(\partial_b f^0_n)\Omega^d_n\,, \quad (4)$$

where $\partial_b = \frac{\partial}{\partial k_b}$, f^0_n is the equilibrium Fermi–Dirac distribution for the nth band, and Ω^d_n represents the component of Berry curvature for the nth band along k_d in momentum space. It is a well-established principle that the simultaneous presence of time-reversal and inversion symmetries imposes a restriction of zero Berry curvature across the entire BZ, precluding the occurrence of the nonlinear Hall effect. Here, in bilayer ferroelectric Bi, the manifestation of in-plane polarization inherently gives rise to non-zero Berry curvatures, which is a prerequisite for the emergence of a nonlinear anomalous Hall current.

We present the Berry curvature-resolved band structures in Fig. 4 for two topologically trivial configurations, $\mathcal{S}[0.0, 0.0]$ and $\mathcal{S}[0.3, 0.0]$, and a nontrivial configuration, $\mathcal{S}[0.4, 0.0]$. These configurations exhibit distinct distributions of Berry curvatures. By comparing Figs. 4(a) and 4(b) with Fig. 4(c), a pronounced reversal in the sign of

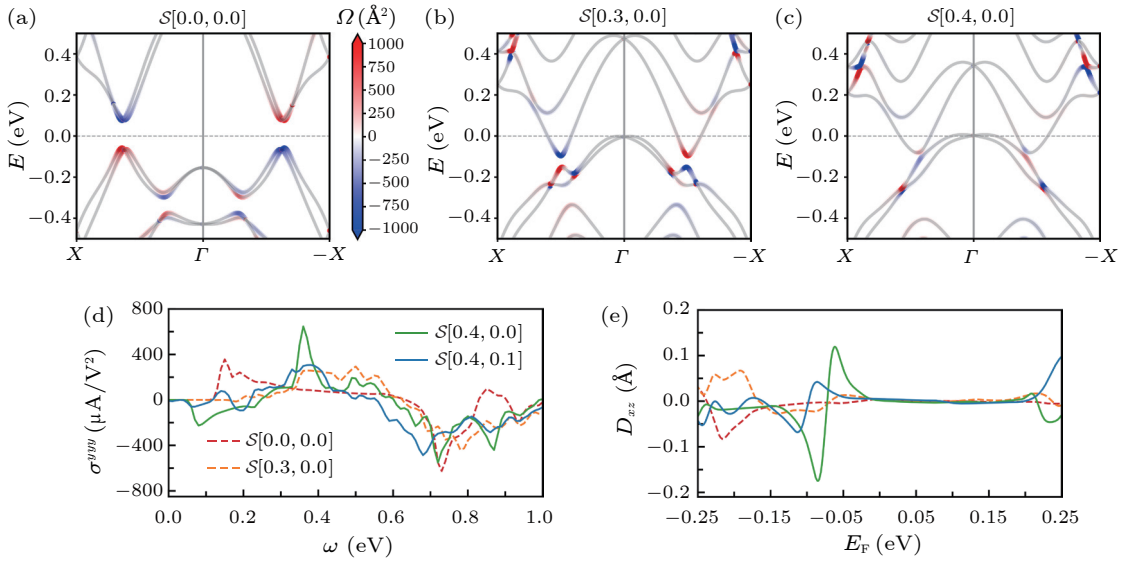

Fig. 4. Berry curvature-resolved band structures for (a) $\mathcal{S}[0.0, 0.0]$, (b) $\mathcal{S}[0.3, 0.0]$, and (c) $\mathcal{S}[0.4, 0.0]$. (d) Shift current spectra of representative configurations with VBM chosen as the zero energy. (e) Berry curvature dipole component D_{xz} as a function of E_F. For each configuration, $E_F = 0$ corresponds to its own intrinsic undoped value calculated with DFT.

the Berry curvature becomes evident near the k-points of gap closure. These results highlight that interlayer sliding can not only induce a topological phase transition but also greatly modulate the band structure and thus the Berry curvature distribution.

The shift current spectra for four different configurations are displayed in Fig. 4(d). In the low-frequency range ($\omega < 0.2$ eV), there is a pronounced difference between the topologically trivial configurations, i.e., $\mathcal{S}[0.0, 0.0]$ and $\mathcal{S}[0.3, 0.0]$, and the nontrivial configurations $\mathcal{S}[0.4, 0.0]$ and $\mathcal{S}[0.4, 0.1]$. Notably, the nontrivial configurations exhibit negative values at lower frequencies. However, in the higher frequency range ($\omega > 0.2$ eV), while the frequencies corresponding to the maximum peaks differ, the overall amplitudes and trends are quite similar across all configurations. Of particular interest is the nontrivial configuration $\mathcal{S}[0.4, 0.0]$, which reaches a peak shift current value of 650 μA/V^2 near $\omega = 0.36$ eV, a value significantly higher than that observed in many other ferroelectric materials [50 μA/V^2 in $PbTiO_3$ and 100 μA/V^2 in GeS].[61,62]

We further quantify the Berry curvature dipole D_{xz}, which scales with the transverse Hall voltage along the y-axis for an input current applied along the x-axis. The results for several representative configurations are presented as a function of the Fermi level (E_F) in Fig. 4(e). It is noted that for each configuration, $E_F = 0$ corresponds to the intrinsic undoped value computed with DFT. The D_{xz} spectra vary significantly among the bilayer configurations. Within a relatively narrow energy window of 0.1 eV around E_F, the topologically trivial configuration $\mathcal{S}[0.0, 0.0]$ exhibits minimal changes, while $\mathcal{S}[0.3, 0.0]$ undergoes more pronounced variations. This can be understood by comparing their band structures [see Figs. 4(a) and 4(b)], where the valence bands at the Γ point in $\mathcal{S}[0.3, 0.0]$ are at higher energies, contributing more states near the Fermi level. Interestingly, the topologically nontrivial configuration $\mathcal{S}[0.4, 0.0]$ yields much larger D_{xz} values, reaching ≈ 0.2 Å, which is higher than the values of ≈ 0.1 Å in WTe_2 and $MoTe_2$.[63] However, further sliding along the y-axis results in smaller D_{xz} values in $\mathcal{S}[0.4, 0.1]$. Overall, D_{xz} profiles of all configurations show strong variations in both sign and magnitude. This suggests that the seemingly "gentle" lateral shift in real space actually can induce unexpectedly large changes in band dispersion and band inversion in momentum space, leading to dramatic changes in the nonlinear anomalous Hall current. These findings underscore the sensitivity of the Berry curvature dipole to structural distortions, offering new opportunities for tuning nonlinear transport properties in bilayer systems.

In conclusion, we demonstrate that a sliding-induced $\mathbb{Z}_2$ topological phase transition is achievable in bilayer ferroelectric bismuth. Counterintuitively, a gentle lateral shift can result in pronounced modulations in the atomic buckling and band structures, driving band gap closure and band inversion that underlie the electronic topological transition. The established topological phase diagram, mapped with respect to sliding in all possible 2D directions, reveals that sliding can induce successive trivial-nontrivial-trivial phase transitions. This provides a deterministic and energy-efficient pathway to configure the quantum spin Hall insulator phase and its symmetry-protected edge states. The Bi bilayer, featuring sliding-tunable ferroelectricity, band topology, and metallicity, offers a unique platform for exploring geometric currents arising from both interband and intraband geometric quantities of electronic bands. Our DFT calculations further reveal that the nontrivial polar metal state supports a substantial shift current response. Additionally, the sign and magnitude of the Berry curvature dipole, and consequently the nonlinear anomalous Hall current, are highly sensitive to the direction and magnitude of sliding, en-

abling precise tuning of the anomalous Hall effect. We suggest that bilayer bismuth is a promising platform for manipulating multiple types of geometrical currents, both deeply rooted in Berry phase, for nonvolatile multistate memory applications.

Acknowledgments. Z.Q. and S.L. acknowledge the supports from Westlake Education Foundation. The computational resource is provided by Westlake HPC Center. H.W. acknowledges the support provided by the National Natural Science Foundation of China (Grant No. 12304049). Z.Q. acknowledges the help from Yudi Yang and Yihao Hu during the preparation of the manuscript.

References

[1] Duong D L, Yun S J, and Lee Y H 2017 *ACS Nano.* **11** 11803
[2] Burch K S, Mandrus D, and Park J G 2018 *Nature* **563** 47
[3] Wu M 2021 *ACS Nano* **15** 9229
[4] Wang C, You L, Cobden D, and Wang J 2023 *Nat. Mater* **22** 542
[5] Zhao J, Li L, Li P *et al.* 2025 *Nature* **639** 354
[6] Wu M, Burton J D, Tsymbal E Y, Zeng X C, and Jena P 2013 *Phys. Rev. B* **87** 081406
[7] Feng J, Qian X, Huang C W, and Li J 2012 *Nature Photon.* **6**866
[8] Nahas Y, Prokhorenko S, Zhang Q, Govinden V, Valanoor N, and Bellaiche L 2020 *Nat. Commun.* **11** 5779
[9] Jiang X, Kang L, Wang J, and Huang B 2023 *Phys. Rev. Lett.* **130** 256902
[10] Sauer M O, Taghizadeh A, Petralanda U, Ovesen M, Thygesen K S, Olsen T, Cornean H, and Pedersen T G 2023 *npj Comput. Mater.* **9** 35
[11] Liang Y, Mao N, Dai Y, Kou L, Huang B, and Ma Y 2021 *npj Comput. Mater.* **7** 172
[12] Li X, Qin B, Wang Y *et al.* 2024 *Nat. Commun.* **15** 10921
[13] Wu F, Li L, Xu Q *et al.* 2023 *Chin. Phys. Lett.* **40** 047303
[14] Yankowitz M, Chen S, Polshyn H *et al.* 2019 *Science* **363** 1059
[15] Sharpe A L, Fox E J, Barnard A W, Finney J, Watanabe K, Taniguchi T, Kastner M A, and Goldhaber-Gordon D 2019 *Science* **365** 605
[16] Liu X, Hao Z, Khalaf E *et al.* 2020 *Nature* **583** 221
[17] Bistritzer R and MacDonald A H 2011 *Phys. Rev. B* **84** 035440
[18] Wang Z F, Liu F, and Chou M Y 2012 *Nano Lett.* **12** 3833
[19] Cao Y, Fatemi V, Fang S, Watanabe K, Taniguchi T, Kaxiras E, and Jarillo-Herrero P 2018 *Nature* **556** 43
[20] Chen G, Sharpe A L, Gallagher P *et al.* 2019 *Nature* **572** 215
[21] Chen G, Jiang L, Wu S *et al.* 2019 *Nat. Phys.* **15** 237
[22] Shimazaki Y, Schwartz I, Watanabe K, Taniguchi T, Kroner M, and Imamoğlu A 2020 *Nature* **580** 472
[23] Cao Y, Fatemi V, Demir A *et al.* 2018 *Nature* **556** 80
[24] Jin C, Regan E C, Yan A *et al.* 2019 *Nature* **567** 76
[25] Tran K, Moody G, Wu F *et al.* 2019 *Nature* **567** 71
[26] Li L and Wu M 2017 *ACS Nano* **11** 6382
[27] Ji J, Yu G, Xu C, and Xiang H J 2023 *Phys. Rev. Lett.* **130** 146801
[28] Miao L P, Ding N, Wang N, Shi C, Ye H Y, Li L, Yao Y F, Dong S, and Zhang Y 2022 *Nature Mater.* **21** 1158
[29] Yasuda K, Wang X, Watanabe K, Taniguchi T, and Jarillo-Herrero P 2021 *Science* **372** 1458
[30] Stern M V, Waschitz Y, Cao W, Nevo I, Watanabe K, Taniguchi T, Sela E, Urbakh M, Hod O, and Shalom M B 2021 *Science* **372** 1462
[31] Woods C R, Ares P, Nevison-Andrews H *et al.* 2021 *Nat. Commun.* **12** 347
[32] Rogée L, Wang L, Zhang Y, Cai S, Wang P, Chhowalla M, Ji W, and Lau S P 2022 *Science* **376** 973
[33] Son Y W, Choi S M, Hong Y P, Woo S, and Jhi S H 2011 *Phys. Rev. B* **84** 155410
[34] Ren Y, Ke S, Lou W K, and Chang K 2022 *Phys. Rev. B* **106** 235302
[35] Xu H, Zhou J, Wang H, and Li J 2020 *J. Phys. Chem. Lett.* **11** 6119
[36] Xiao J, Wang Y, Wang H *et al.* 2020 *Nat. Phys.* **16** 1028
[37] Wang H and Qian X 2019 *npj Comput. Mater.* **5** 119
[38] Du S, Tang P, Li J, Lin Z, Xu Y, Duan W, and Rubio A 2020 *Phys. Rev. Res.* **2** 022025
[39] Singh S, Kim J, Rabe K M, and Vanderbilt D 2020 *Phys. Rev. Lett.* **125** 046402
[40] Gou J, Bai H, Zhang X *et al.* 2023 *Nature* **617** 67
[41] Peng B, Lange G F, Bennett D, Wang K, Slager R J, and Monserrat B 2024 *Phys. Rev. Lett.* **132** 116601
[42] Liu Z, Liu C X, Wu Y S, Duan W H, Liu F, and Wu J 2011 *Phys. Rev. Lett.* **107** 136805
[43] Guo P J, Lu X Q, Ji W, Liu K, and Lu Z Y 2020 *Phys. Rev. B* **102** 041109
[44] Kou L, Niu C, Fu H, Ma Y, Yan B, and Chen C 2018 *Appl. Phys. Lett.* **112** 243103
[45] Yang L, Li L, Yu Z M, Wu M, and Yao Y 2024 *Phys. Rev. Lett.* **133** 186801
[46] Giannozzi P, Baroni S, Bonini N *et al.* 2009 *J. Phys. Condens. Matter* **21** 395502
[47] Giannozzi P, Andreussi O, Brumme T *et al.* 2017 *J. Phys. Condens. Matter* **29** 465901
[48] Perdew J P, Burke K, and Ernzerhof M 1996 *Phys. Rev. Lett.* **77** 3865
[49] Garrity K F, Bennett J W, Rabe K M, and Vanderbilt D 2014 *Comput. Mater. Sci.* **81** 446
[50] van Setten M, Giantomassi M, Bousquet E, Verstraete M, Hamann D, Gonze X, and Rignanese G M 2018 *Comput. Phys. Commun.* **226** 39
[51] Krukau A V, Vydrov O A, Izmaylov A F, and Scuseria G E 2006 *J. Chem. Phys.* **125** 224106
[52] Marzari N, Mosto A. A, Yates J R, Souza I, and Vanderbilt D 2012 *Rev. Mod. Phys.* **84** 1419
[53] Pizzi G, Vitale V, Arita R *et al.* 2020 *J. Phys.: Condens. Matter.* **32** 165902
[54] Xiao C, Wang F, Yang S A, Lu Y, Feng Y, and Zhang S 2018 *Adv. Funct. Mater.* **28** 1707383
[55] Sui F, Li H, Qi R *et al.* 2024 *Nat. Commun.* **15** 3799
[56] Kraut W and von Baltz R 1979 *Phys. Rev. B* **19** 1548
[57] Sipe J E and Shkrebtii A I 2000 *Phys. Rev. B* **61** 5337
[58] Jin K H, Oh E, Stania R, Liu F, and Yeom H W 2021 *Nano Lett.* **21** 9468
[59] Sodemann I and Fu L 2015 *Phys. Rev. Lett.* **115** 216806
[60] Morimoto T, Zhong S, Orenstein J, and Moore J E 2016 *Phys. Rev. B* **94** 245121
[61] Young S M and Rappe A M 2012 *Phys. Rev. Lett.* **109** 116601
[62] Rangel T, Fregoso B M, Mendoza B S, Morimoto T, Moore J E, and Neaton J B 2017 *Phys. Rev. Lett.* **119** 067402
[63] You J S, Fang S, Xu S Y, Kaxiras E, and Low T 2018 *Phys. Rev. B* **98** 121109